BioCombs4Nanofibers

Project BioCombs4Nanofibers

D3.1 Formation Mechanisms of LIPSS and achievable structure size

Work completed in Period	from	**01.10.2019**	to	**30.06.2020**
Deliverable completed and released		**29.06.2020** **George D. Tsibidis, Jörn Bonse, Johannes Heitz**		

Contents

Table of Contents

1. Introduction

Overall goal: D3.1 has the aim to create a public scientific report on the formation mechanisms of LIPSS reporting on achievable structure sizes for the materials under investigation.

Laser surface patterning can be classified in approaches based on *self-organized* laser-irradiated structures and *direct laser-inscribed* structures. Self-organized means here that although the surface is irradiated using a homogeneous spatial beam profile in a spot or scanning geometry, the resulting surface topography features characteristic (quasi-) periodic surface morphologies. The self-organized surface structures may consist of microstructures, nanostructures, or hybrid variants. All these different structures resemble surface morphologies found in nature and, therefore, can be considered as "*biomimetic*". For a review of the types of structures fabricated after irradiating solids with pulsed lasers see Refs. [1,2].To allow fabrication of these structures in a systematic way, a thorough

knowledge of how laser interacts with solids and the underlying physical mechanisms need to be accurately described.

In the following sections, the formation mechanisms of different types of *laser-induced periodic surface structures* (LIPSS) are discussed in more detail. In Section 2, the laser-matter interaction mechanisms are briefly summarized, while Section 3 an overview of the most common types of LIPSS, i.e. *Ripples*, *Grooves*, and *Spikes* and their formation mechanisms are provided. Then term *Ripples* includes so-called *low-spatial frequency LIPSS* (LSFL) with spatial periods close to the irradiation wavelength λ, and *high-spatial frequency LIPSS* (HSFL) with periods much smaller than the wavelength ($<\lambda/2$). In Section 4, the achievable size of these surface structures is provided. Section 5 presents a new predictive machine learning modelling approach, which will be explored in the BioCombs4Nanofibers project.

This document represents mostly an excerpt of the invited **review article [1] published within the BioCombs4Nanofibers project on June 21st 2020.**

2. Laser-Matter Interaction

2.1 Laser irradiation and excitation

To understand the physical mechanism that accounts for the surface modification upon irradiation of solids with femtosecond (ps) pulsed lasers, we perform a multiscale modelling of the processes that describe laser beam energy absorption and response of the material. While a generalisation can follow to describe response of any type of material, the emphasis in this report will be drawn on surface modification mechanisms after irradiation of *metals* (i.e. stainless steel). The multiscale theoretical model that is presented comprises the following components: (i) a term that describes energy absorption, (ii) a term that describes electron excitation, (iii) a heat transfer component that accounts for electron-lattice thermalisation through particle dynamics and heat conduction and carrier-phonon coupling, and (iv) a hydrodynamics component that describes fluid dynamics followed by a mass removal and re-solidification process in areas where a phase transition occurs. In principle, the processes start after some fs, they continue to mechanisms that complete after some picoseconds (ps) while others require more time and they last up to the nanosecond (ns) regime.

2.2 Relaxation processes

The *two-temperature model* (TTM) constitutes the standard theoretical method to investigate laser-matter interaction of solids upon ultrashort laser irradiation, which assumes an instantaneous electron excitation during the laser pulse that produces fast electron thermalisation on the femtosecond timescale (see Ref.[1]). The TTM is implemented by the following set of coupled differential equations that describe the absorption of optical radiation by the electrons and the energy transfer between the electron and lattice subsystems.

$$\begin{aligned} C_e \frac{\partial T_e}{\partial t} &= \vec{\nabla}\left(k_e \vec{\nabla} T_e\right) - g(T_e - T_L) + S \\ C_L \frac{\partial T_L}{\partial t} &= \vec{\nabla}\left(k_L \vec{\nabla} T_L\right) + g(T_e - T_L) \end{aligned} \quad (1)$$

T_e and T_L are the electron and lattice temperatures, k_e and k_L (~0.01k_e and therefore, that term could even be neglected) stand for the electron and lattice heat conductivities, C_e and C_L correspond to the electron and lattice heat capacities, and g is the electron-phonon coupling

strength. The heat source *S* in a Cartesian system of coordinates (*x,y,z*) is modelled by assuming a Gaussian temporal profile and it has the following (simplified, to first approximation) form

$$S(\mathrm{x},\mathrm{y},\mathrm{z},\mathrm{t}) = \frac{\alpha(1-R)\sqrt{4\log 2}\varphi_0}{\sqrt{\pi}\tau_p}\exp\left(-4\log 2\left(\frac{t-3\tau_p}{\tau_p}\right)^2\right)\exp(-\alpha z)\exp\left[-\left(\frac{x+y}{w_0}\right)^2\right], \qquad (2)$$

where τ_p is the pulse duration, φ_0 is the peak fluence, α and R stand for the absorption coefficient and the surface reflectivity, respectively, of the irradiated material and w_0 is the 1/*e*-Gaussian laser irradiation spot radius. For the sake of simplicity, it is assumed that optical properties (α, R) do not have a spatio-temporal variation.

2.3 Phase transition and resolidification

In order to describe the thermal response of the laser-irradiated material after electron-phonon relaxation processes, it is important to model heat transfer into the material, possible phase transitions and solidification. Since the laser irradiation conditions used in the simulations are sufficient to melt a portion of the material (once the lattice temperature reaches the melting temperature T_{melt}), the induced phase change has to be thoroughly analysed. Upon thermal relaxation due to electron-phonon scattering, the characteristic spatial modulation will be projected on the lattice system and fluid dynamics (when the material undergoes a phase transition) leading eventually to a rippled surface topography profile when the resolidification process ends [1]. The material that undergoes melting is assumed to be an incompressible Newtonian fluid and its dynamics is described by the *Navier-Stokes equations* [1]. Molten material can be transiently subjected to thermocapillary forces that are driven by local temperature gradients (e.g. Marangoni effect, convection rolls, etc.). Moreover, modulated ablation can contribute to the generation of a corrugated surface.

3. Formation mechanisms of LIPSS

To provide a detailed description of the physical origin of LIPSS formation as well as the quantitative features of the induced self-assembled structures on the surface of the irradiated material upon excitation with ultrashort pulsed lasers, a thorough investigation of the underlying multiscale phenomena that take place is required. While the precise physical mechanism for the origin of LIPSS is still a point of ongoing scientific discussions (but as mentioned above appears to be of electromagnetic origin), one process that undoubtedly occurs is a transient phase transition, i.e., melting, that eventually leads to a surface modification.

3.1 Ripples

Various approaches were developed to explain the formation of LIPSS. Below, we present an overview of the most successful methods.

3.1.1 SPP mechanism to explain ripple formation

The most simple (analytical) model for the formation of ripples is based on the idea of a coherent interaction of the incident laser radiation with the resonantly driven electron system

of the solid – a phenomenon known as *Surface Plasmon Polariton* (SPP). The interference of the laser field with that of the SPP can then lead to a spatial modulation of the absorbed energy, that finally imposes a periodic surface corrugation in the form of near-wavelength-sized ripples (LSFL) being perpendicular oriented to the laser beam polarization [1,2].
The procedure that leads to the rippled pattern following irradiation of the material with multiple laser pulses is the following:

- the first pulse irradiates a flat surface and it is assumed to melt/ablate (depending on the laser intensity/fluence) a part of the material - leading to the formation of a crater and humps at the edges on the surface of the heated zone due to mass displacement [3,4]. As the first pulse irradiates a flat surface with no corrugations, formation of periodic structures is not expected to occur [5].
- the second pulse irradiates the previously formed profile and, therefore, the spatial symmetry of the surface breaks; that may allow the excitation of SPPs if certain requirements on the optical surface properties are fulfilled [6]. The coupling of the electric field of the incident laser beam with the induced SPP produces a nonuniform, spatially periodic distribution of the absorbed energy (of periodicity and orientation determined by the density of excited carriers and the efficacy factor). The induced spatial modulation of the absorbed energy is introduced as a sinusoidal function of periodicity; the periodic variation of the absorbed energy leads to a periodic excited electron density distribution as explained above. It is noted, though, that the computation of the amount of the absorbed energy at each position requires the evaluation of the energy deposition on a curved surface [3,7]. Therefore, appropriate computational schemes have been developed to compute the absorbed energy on each point of the curved surface [3]. The spatially modulated electron energy distribution is then in a second step transferred to the lattice system of the material and subsequently, upon phase transition (melting and ablation), fluid transport and resolidification processes, LIPSS are formed as periodic surface corrugations.
- In an iterative fashion, each subsequent laser pulse irradiates a periodic pattern that has been created in the previous step; it is noted that the depth of the surface profile is increased with increasing number of laser pulses (*NP*) [7,8].

3.1.2 Sipe's theory

A more general analytic approach was developed by John E. Sipe at the university of Toronto during the eighties of the past century. This first-principles theory [5] uses the *Green's formalism* to develop the electromagnetic theory of the absorption of a microscopically rough surface from *Maxwell's equations*. It inherently includes the possible excitations of SPP and represents the currently most widely accepted theory of LIPSS, although inter-pulse feedback by multiple pulse irradiations is explicitly not included. It is, nevertheless, very successful to predict spatial periods of LIPSS for a given material (dielectric permittivities, surface roughness) and irradiation parameters (wavelength, angle of incidence, polarization direction) and can be used in a simplified form [9].

3.1.3 FDTD-Simulations

For completeness, *finite-difference time-domain* (FDTD) simulations should be mentioned as powerful method for studying the origin of LIPSS on basis of electromagnetic scattering and absorption phenomena [10,11]. For dielectrics, it allowed to identify a shared origin between sub-wavelength HSFL and so-called *volume structures* [12,13], The FDTD method was successfully coupled with the TTM and Navier-Stokes equations [14].

3.1.4 Polymers

Further investigations have shown that ripple formation is a general phenomenon, observed practically always on solid or liquid surfaces after laser irradiation with polarized light within certain ranges of laser parameters. Laser pulse lengths in the order of some ns, fluences well below the ablation threshold, and a large number of laser pulses have to be applied to induce LIPSS formation on polymer surfaces, like polyethylene terephthalate (PET) or polystyrene (PS). The formed nanostructures depend on the laser wavelength, λ, as well as the angle of incidence, θ, of the laser beam [15-17]. For *s*-polarization, the lateral periodicity Λ is given by

$$\Lambda = \frac{\lambda}{n_{eff} - sin\theta} \qquad (3)$$

where n_{eff} is the effective refractive index, which lies between the index of air (≈1) and the index of the polymer. The direction of the ripples in case of polymers is parallel to the polarization direction. The structure periodicity Λ can be varied by means of different irradiation parameters, but not independently from the structure height, *h*. The aspect ratio of the ripples (i.e., h divided by half of Λ) is typically around 0.5.

3.2 Microgrooves

Grooves manifest as quasi-periodic self-organized ablation lines with supra-wavelength periods, for optical laser radiation typically on the micrometer scale. A key feature for groove formation in metals and semiconductors is an originally surface profile covered with sub-wavelength ripples. These are physical modes that are solutions of the Navier-Stokes equations, however, propagation of hydrothermal waves that lead to stable structures upon solidification are predicted for particular values of the frequency of the produced waves that may explain the supra-wavelength character of grooves (Fig. 1).

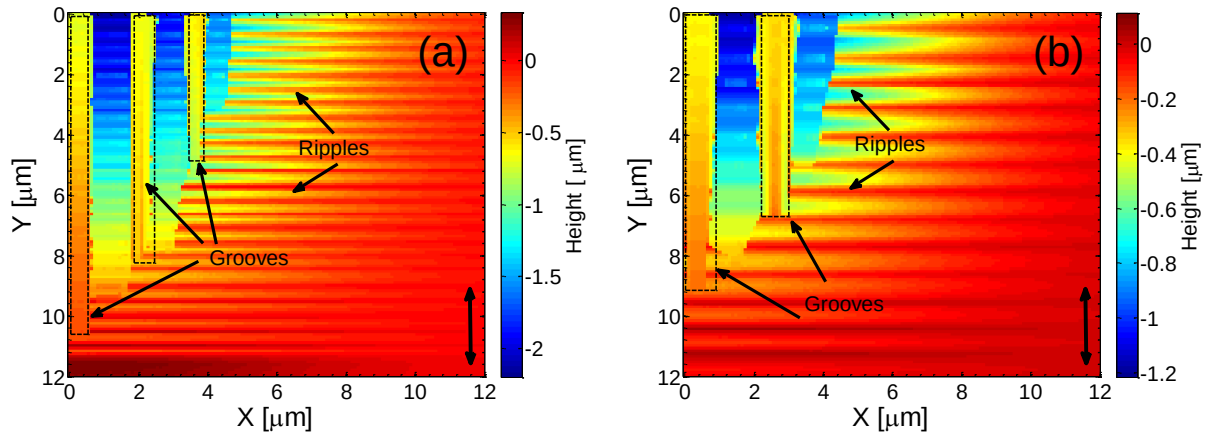

Figure 1: Ripples and Grooves on Steel for (a) 513 nm and (b) 1026 nm, (pulse duration τ_p=170 fs, fluence φ_0=0.5 J/cm²)

3.3 Microspikes

Simulations predict the microspikes formation to convection-roll driven hydrodynamic phenomena [1,2]. More specifically, simulations show that spike-related protrusions require an originally built groove-covered profile. For metals and semiconductors in which grooves are decorated with pseudoripples, further irradiation and increase of energy dose leads to gradual diminishing of the pseudoripples and increase of the height of grooves.

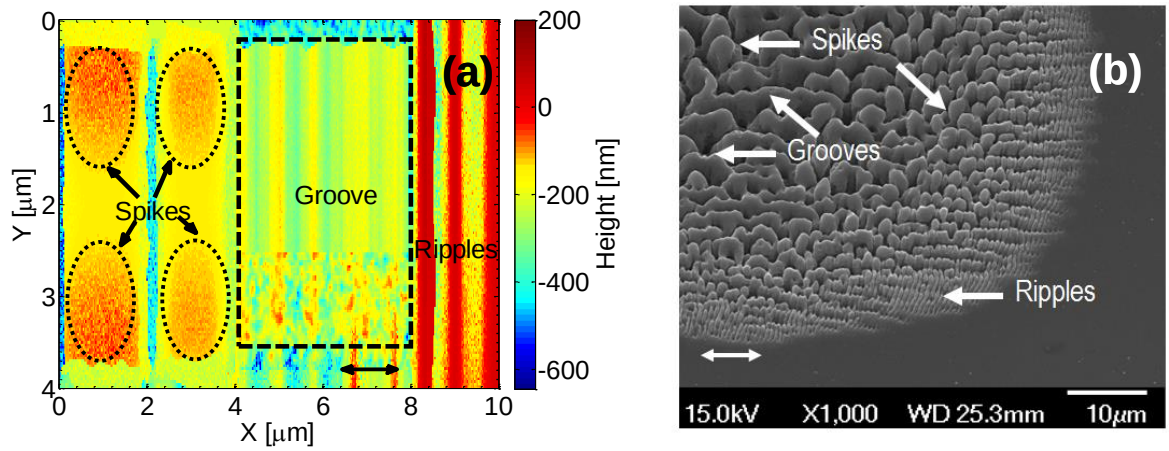

Fig. 2: (a) Surface pattern on Silicon following irradiation with 120 laser pulses, (b) Experimental results for 200 laser pulses (Double-ended arrow indicates the laser beam polarization). (Reprinted from Tsibidis et al [18])

4. Minimum achievable structure sizes

Among the different types of LIPSS, if formed, the HSFL structures exhibit the smallest structure sizes. Moreover, the spatial periods of the HSFL exhibit a lower size limit, which may even approach values below 100 nm [19,20]. Different origins were proposed for this lower size limit. In Ref. [1], the electron-phonon coupling process was identified as one limiting factor since the spatially modulated pattern of optical energy can smear out during the transfer of this energy from the electronic system of the solid to its lattice on timescales typically of a few ps. Recent FDTD-simulations coupled to hydrodynamic modelling based on Navier-Stokes equations identified the Marangoni convection instabilities and the minimum melt layer thickness as another limiting effect for fs-laser irradiated metals[14].

Table 1 summarizes the achievable structure size ranges for the materials under investigations in the **BioCombs4Nanofibers** project, i.e., steel, titanium, and polymer materials upon irradiation at wavelength in the UV-NIR spectral range.

Material	LIPSS type	Size range [μm]
Steel	HSFL LSFL Grooves Spikes	(not simulated) 250nm-1000nm 1.5-3.5μm 2-13μm (unpublished results)
Titanium/-alloy	HSFL LSFL Grooves Spikes	0.07 0.12 0.3 – 1.1 1 – 4 4 – 15
Polymer	HSFL LSFL Grooves Spikes	0.08 – 0.14 0.13 – 1.1 Not observed 1 – 10

Table 1: Achievable structure size ranges, summarized from the experiments and simulations.

5. A Machine learning based approach towards a systematic and fast LIPSS fabrication

Predictive modelling represents an emerging field that combines existing and novel methodologies aimed to rapidly understand physical mechanisms and concurrently develop new materials, processes and structures. In our study [9], previously-unexplored predictive modelling in a key-enabled technology, the laser-based manufacturing, aims to automate and forecast the effect of laser processing on material structures. The focus is centered on the performance of representative statistical and machine learning algorithms in predicting the outcome of laser processing on a range of materials. Our results can set the basis for a systematic methodology towards reducing material design, testing and production cost via the replacement of expensive trial-and-error based manufacturing procedure with a precise pre-fabrication predictive tool [21]. Figure 3 illustrates simulated and data produced through machine learning based approaches towards estimating laser conditions to produce specific types of structures.

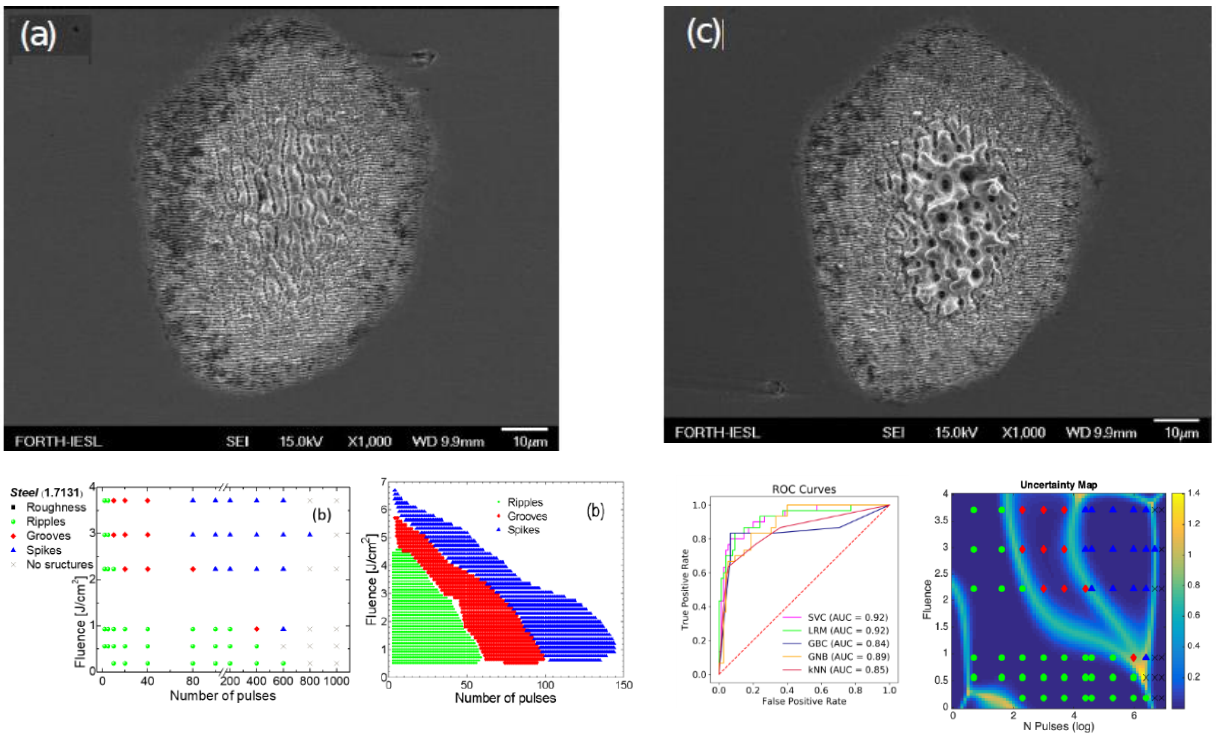

Fig. 3: Surface modification on Stainless Steel: SEM images of patterned surfaces with (a) ripples, (b) grooves and ripples. (c) mapping that illustrates experimental (left) and simulated (right) data for various types of structures, (d) Performance assessment of several predictive models on experimental data for all studied materials (left); Uncertainty quantification for the studied materials using logistic regression as predictive model (right).

6. Conclusions

The current deliverable D3.1 “Formation Mechanisms of LIPSS and achievable structure size” is related to the activities in Task 3.1 towards advancement of the state of the art of modelling laser-matter interaction and LIPSS modelling. The objective of the work was to provide a the framework that will allow a systematic fabrication of specific surface pattern features via an improved understanding of the (multiscale) physical phenomena that occur

after irradiation of solids with femtosecond pulses. A thorough knowledge of the physical processes is expected to enable the prediction of the irradiation schemes that lead to a target surface feature pattern for a specific material.

Finally, to show connection with other tasks of the project, the developed computational code is aimed to complement the experimental activities towards the design of a reliable and accurate formation of tailored hierarchical surface textures with desired fabrication.

This report has been published as a public report (PDF) entitled “Formation Mechanisms of LIPSS” in the Dissemination section of the web-site of the **BioComb4Nanofibers** project (http://biocombs4nanofibers.eu).

7. References

[1] E. Stratakis, J. Bonse, J. Heitz, J.Siegel, G.D.Tsibidis, E.Skoulas, A. Papadopoulos, A.Mimidis, A.-C. Joel, P. Comann, J. Kruger, C.Florian, Y. Fuentes-Edfuf, J. Solis, W. Baumgartner, Materials Science and Engineering: R: Reports **141**, 100562 (2020).

[2] J. Bonse, S. Höhm, S. V. Kirner, A. Rosenfeld, and J. Krüger, IEEE Journal of Selected Topics in Quantum Electronics **23**, 9000615 (2017).

[3] G. D. Tsibidis, M. Barberoglou, P. A. Loukakos, E. Stratakis, and C. Fotakis, Physical Review B **86**, 115316 (2012).

[4] G. D. Tsibidis, E. Skoulas, A. Papadopoulos, and E. Stratakis, Physical Review B **94**, 081305(R) (2016).

[5] J. E. Sipe, J. F. Young, J. S. Preston, and H. M. van Driel, Physical Review B **27**, 1141 (1983).

[6] T. J. Y. Derrien, J. Krüger, and J. Bonse, Journal of Optics **18**, 115007 (2016).

[7] G. D. Tsibidis and E. Stratakis, Journal of Applied Physics **121**, 163106 (2017).

[8] M. Huang, F. L. Zhao, Y. Cheng, N. S. Xu, and Z. Z. Xu, ACS Nano **3**, 4062 (2009).

[9] J. Bonse, M. Munz, and H. Sturm, Journal of Applied Physics **97**, 013538 (2005).

[10] J. Z. P. Skolski, G. R. B. E. Romer, J. V. Obona, V. Ocelik, A. J. H. in 't Veld, and J. T. M. De Hosson, Physical Review B **85**, 075320 (2012).

[11] A. Rudenko, PhD Thesis, Université de Lyon, (2017).

[12] R. Buschlinger, S. Nolte, and U. Peschel, Physical Review B **89** (2014).

[13] A. Rudenko, J. P. Colombier, S. Hohm, A. Rosenfeld, J. Kruger, J. Bonse, and T. E. Itina, Scientific Reports **7**, 12306 (2017).

[14] A. Rudenko, A. Abou-Saleh, F. Pigeon, C. Mauclair, F. Garrelie, R. Stoian, and J. P. Colombier, Acta Mater **194**, 93 (2020).

[15] E. Rebollar, S. Pérez, J. J. Hernández, I. Martín-Fabiani, D. R. Rueda, T. A. Ezquerra, and M. Castillejo, Langmuir **27**, 5596 (2011).

[16] S. Pérez, E. Rebollar, M. Oujja, M. Martín, and M. Castillejo, Applied Physics A **110**, 683 (2013).

[17] D. Baeuerle, E. Arenholz, V. Svorcik, J. Heitz, B. Luk'yanchuk, and N. Bityurin, *Laser-induced surface modifications, structure formation, and ablation of organic polymers* (SPIE, 1995), Vol. 2403, Photonics West '95, Page 312.

[18] G. D. Tsibidis, C. Fotakis, and E. Stratakis, Physical Review B **92**, 041405(R) (2015).

[19] J. Heitz, E. Arenholz, D. Bauerle, R. Sauerbrey, and H. M. Phillips, Applied Physics A-Materials Science & Processing **59**, 289 (1994).

[20] J. Bonse, S. Höhm, A. Rosenfeld, and J. Krüger, Applied Physics A-Materials Science & Processing **110**, 547 (2013).

[21] M. C. Velli, G. D. Tsibidis, M. A., S. E., Y. Pantazis, and E. Stratakis, *(Preprint: Arxiv: https://arxiv.org/abs/2006.07686*) (2020).